Received: 11 May 2016 | Revised: 14 January 2017 | Accepted: 15 January 2017

DOI 10.1002/tox.22397

RESEARCH ARTICLE

WILEY ENVIRONMENTAL TOXICOLOGY

Effects of silver nanoparticles on the interactions of neuron- and glia-like cells: Toxicity, uptake mechanisms, and lysosomal tracking

I-Lun Hsiao | Yi-Kong Hsieh | Chun-Yu Chuang | Chu-Fang Wang | Yuh-Jeen Huang

Department of Biomedical Engineering and Environmental Sciences, National Tsing Hua University, Hsinchu 30013, Taiwan

Correspondence
Yuh-Jeen Huang, No. 101, Section 2, Kuang-Fu Road, Hsinchu, Taiwan 30013.
Email: yjhuang@mx.nthu.edu.tw

Funding information
Ministry of Science and Technology (MOST), Taiwan, Grant Number: 103-2221-E-007-006-MY3

Abstract

Silver nanoparticles (AgNPs) are commonly used nanomaterials in consumer products. Previous studies focused on its effects on neurons; however, little is known about their effects and uptake mechanisms on glial cells under normal or activated states. Here, ALT astrocyte-like, BV-2 microglia and differentiated N2a neuroblastoma cells were directly or indirectly exposed to 10 nm AgNPs using mono- and co-culture system. A lipopolysaccharide (LPS) was pretreated to activate glial cells before AgNP treatment for mimicking NP exposure under brain inflammation. From mono-culture, ALT took up the most AgNPs and had the lowest cell viability within three cells. Moreover, AgNPs induced H_2O_2 and NO from ALT/activated ALT and BV-2, respectively. However, AgNPs did not induce cytokines release (IL-6, TNF-α, MCP-1). LPS-activated BV-2 took up more AgNPs than normal BV-2, while the induction of ROS and cytokines from activated cells were diminished. Ca^{2+}-regulated clathrin- and caveolae-independent endocytosis and phagocytosis were involved in the AgNP uptake in ALT, which caused more rapid NP translocation to lysosome than in macropinocytosis and clathrin-dependent endocytosis-involved BV-2. AgNPs directly caused apoptosis and necrosis in N2a cells, while by indirect NP exposure to bottom chamber ALT or BV-2 in Transwell, more apoptotic upper chamber N2a cells were observed. Cell viability of BV-2 also decreased in an ALT–BV-2 co-culturing study. The damaged cells correlated to NP-mediated H_2O_2 release from ALT or NO from BV-2, which indicates that toxic response of AgNPs to neurons is not direct, but indirectly arises from AgNP-induced soluble factors from other glial cells.

KEYWORDS

central nervous system, coculture, cytokines, reactive oxygen and nitrogen species, silver nanoparticles, uptake mechanisms

1 | INTRODUCTION

Silver nanoparticles (AgNPs) are the most commonly used nanomaterials in consumer products. Because of their antimicrobial properties, AgNPs are often used in textiles, disinfecting/antivirus sprays and food containers.[1] They also have further applications in biomedical fields, for instance, in clinical diagnostics and wound dressings.[2,3] Thus, intended or unintended human exposure to AgNPs is increasing.

In vivo studies have found that AgNPs would translocate into the central nervous system (CNS),[4–7] which might be directly through the olfactory bulb[8] or indirectly via penetration of blood-brain barrier (BBB).[7,9] Though the rate of NP translocation to the brain is relatively low, they may exhibit a longer half-life in brain than in other organs.[5,10] AgNPs can be deposited in various regions of the brain, such as the cerebral cortex, hippocampus, and cerebellum[11]; especially in the hippocampus, causing synaptic degeneration in rat,[11] altering oxidative stress and antioxidant defense genes expression in mice,[12] and impairing spatial cognition in rat offspring.[13] Therefore, potential health risks to the brain exist when exposed to AgNPs.

The brain is made up of neurons and glial cells (astrocytes, microglia, and oligodendrocytes). Astrocytes, which account 72–81% in CNS system, supply nutrients (e. g., glutamine, GABA) to neurons and

protect cells from oxidative stress by glutathione production.[14] As specifically immune cells in brain, microglia are in rest state in general. Once neurons are damaged, microglia will be activated and stabilize the damage by engulfing dead cells. However, activated microglia in chronic inflammation keep producing cytokines and chemokines, which leads to neuronal death.[15] Previous *in vitro* neurotoxicity studies on AgNPs mostly focused on the effects of neurons.[16–18] However, relatively few reports discussed the effects of AgNPs on microglia and astrocytes, especially microglia.[19–21]

Recent studies have found that NPs are taken up mainly by astrocytes or microglia, not by neurons.[22,23] Astrocytes are one of BBB components, which are easier to be exposed NP than the other brain cells. Therefore, effects of NPs on glia cells may play more important roles in the mechanisms of NP-induced neurotoxicity. For example, studies have found that TiO_2NP-induced soluble factors (ROS or cytokines release) from microglia might damage neurons.[24,25] However, none of study discussed whether AgNP-mediated soluble factors from astrocyte or microglia damaged neuron indirectly. Moreover, it is essential to study cellular uptake mechanisms and localization of AgNPs in the glia cells because those messages may be related to the toxic responses. For instance, if AgNPs translocated to lysosome via endocytosis pathways, a lysosome-acidic environment promoted more Ag ion release to trigger cellular toxicity.[26] Only one study mentioned that macropinocytosis and endosomal pathways were involved in AgNP-treated astrocytes.[19] On the other hand, as microglia and astrocyte activation occur following almost all CNS pathologies, it is also crucial to know whether AgNPs cause more serious cellular responses under activated state of cells.

In this study, we assumed that the neurons can be damaged by soluble factors (NO, ROS, cytokines) from microglia or astrocytes through high amount of AgNPs uptake by endocytosis pathways. Indirect effects could be enhanced in the activated state of glia cells. To confirm the hypothesis, toxic responses of 10 nm AgNPs were studied in the murine brain astrocyte-like (ALT), immortalized microglia (BV-2) and differentiated neuroblastoma (N2a) cells. The uptake mechanisms of AgNPs and NP-lysosome colocalization in ALT, BV-2, and activated BV-2 were also studied. Indirect effects of AgNPs on N2a or BV-2 were studied via ALT-N2a, BV-2-N2a, and ALT-BV-2 coculture using the Transwell® system. Cell viability, cell death process (N2a), uptake, intracellular ROS, extracellular NO/H_2O_2, and cytokines (IL-6, TNF-α, and MCP-1) release in mono- and coculture were analyzed. The effects of AgNP in inflammatory and activated states of the three cell lines were investigated by coadministration of lipopolysaccharides (LPS).

2 | MATERIALS AND METHODS

2.1 | Nanoparticle source

Obtained from Gold Nanotech, Inc., Taiwan, 10 nm AgNPs were produced by a proprietary molecular beam epitaxy process and did not contain surfactants or stabilizers.[27,28] The AgNPs synthesis procedures are described in Supporting Information (SI). A concentration of AgNPs in stock solution was determined by inductively coupled plasma mass spectrometry (ICP-MS) (Agilent 7500a, CA). Solutions had good stability in storage for at least 6 months at 4°C.

2.2 | Nanoparticle physicochemical characterization

Before characterizing NP in water or cell medium, AgNP stock solution (12 μg mL^{-1}) was first ultrasonicated at 400W for 10 min (DC400H, DELTA new instrument Ltd., Taiwan) to achieve optimal dispersion. The size and morphology of the NPs in stock solution were analyzed using a JEM2100 transmission electron microscope (TEM) (JEOL, Japan). The hydrodynamic size and surface charge of the NPs in water and cell medium [phenol red-free Dulbecco's Modified Eagle's Medium, DMEM) with HEPES and L-glutamine (Gibco® Invitrogen, CA) supplemented with 10% fetal bovine serum (FBS) (Biological Industries, Israel)] was monitored using a Zetasizer Nano ZS apparatus (Malvern Instruments, UK). For measurements, particles were diluted to 3–0.25 μg mL^{-1}. To observe the stability of NPs in cell media, variations in size after 24 and 48 h of incubation were monitored. Free Ag ions in stock solution, which accounted for 2% of solution, has been analyzed by ion-selective electrode in our previous study.[29] Dissolution of AgNPs in cell medium within 48 h was analyzed by UV–Vis spectroscopy. Details of UV–Vis measurements are presented in Supporting Information.

2.3 | Monoculture, LPS treatment, and AgNP exposure

Murine brain astrocyte-like ALT (BCRC 60581, Taiwan), murine microglial BV-2 cells (ATL03001, ICLC, Genova, Italy) and murine neuroblastoma Neuro-2a (N2a) cells (BCRC 60026, Taiwan) were used in the study. N2a cells were cultured in high-glucose DMEM with L-glutamine supplemented with 10% FBS, 1% penicillin–streptomycin (Biological Industries, Israel), and 1% sodium pyruvate (Invitrogen, CA). ALT cells and BV-2 cells were cultured in the same medium as N2a cells, but without 1% sodium pyruvate. For differentiation, N2a cells were treated with 30 μM forskolin and 200 μM isobutylmethylxanthine (IBMX) (Sigma–Aldrich, St. Louis, MO) in DMEM supplemented with 1% FBS for 2 days after 1 day of attachment.[30] Three cell lines were cultivated at 37°C, 5% CO_2 and with 95% relative humidity.

Cells were seeded and attached for 24 h (9×10^3 cells/cm^2 for ALT and BV-2; 5×10^3 cells/cm^2 for N2a). To activate the cells prior to NP treatment, they were pre-treated with LPS from *Escherichia coli* 055:B5 (Sigma–Aldrich, St. Louis, MO) (0.2 μg mL^{-1} for BV-2 cells and 2 μg mL^{-1} for ALT and N2a cells) in serum-free DMEM medium for 6 h. For non-LPS group, cells were incubated only in serum-free medium. AgNPs were first diluted to an indicated concentration (12–0.5 μg mL^{-1}) in DMEM/20%FBS, and then the same volume of NP suspensions as pretreatment use were added to achieve final concentration of LPS (0.1 μg mL^{-1} for BV-2 cells and 1 μg mL^{-1} for ALT and N2a cells) and AgNPs (6–0.25 μg mL^{-1}) in DMEM/10%FBS medium.

2.4 | Co-culture, LPS treatment, and AgNP exposure

For coculture of ALT and N2a/BV-2 and N2a, N2a cells (5×10^3 cells cm^{-2}) were first seeded in the upper chamber (insert) of 24-well

or 6-well Transwell plates [0.4-μm pore size, polyester membrane Transwell (Corning, MA)]. After 24 h of attachment, cells were differentiated by forskolin and IBMX for 2 days. On the third day, ALT cells (9×10^3 cells cm^{-2}) or BV-2 cells (1.6×10^3 cells cm^{-2}) were seeded in separate 24-well or 6-well well plates. After 24-h attachment, the inserts and culture plates which contained differentiated N2a cells and ALT/BV-2, respectively were combined together before following LPS and NP exposure. For ALT and BV-2 coculture, BV-2 cells (1×10^4 cells cm^{-2}) and ALT (9×10^3 cells cm^{-2}) were seeded separately in inserts of the Transwell plates and culture plates, respectively. After 24 h of attachment, the inserts and culture plates were combined together before following up with LPS and NP exposure. Cell density for the three cocultured system was determined by the ratio of initial seeding cells which should be equal to 10% neuron, 9–18% microglia, and 72–81% astrocytes, and which corresponds to the cell ratio in a human brain.[31,32] To induce inflammation responses prior to NP treatment, bottom chamber cells were pre-treated with LPS (0.2 μg mL^{-1} for BV-2-N2a and ALT-BV-2 and 2 μg mL^{-1} for ALT-N2a co-culture system) in serum-free DMEM medium for 6 h. For non-LPS group, cells were incubated only in serum-free medium. Then, the same volume of NP suspensions for pre-treatment use were added to achieve final concentration of LPS (0.1 μg mL^{-1} for BV-2-N2a and ALT-BV-2 coculture system and 1 μg mL^{-1} for ALT-N2a co-culture system) and AgNPs (6, 3, and 1 μg mL^{-1}) in DMEM/10%FBS medium in bottom chamber. In insert, equal volume of fresh DMEM/20%FBS as serum-free medium was added.

2.5 | Cell viability

After 24 and 48 h of AgNP exposure, all NP suspensions were discarded and alamarBlue® (AbD Serotec, Kidlington, UK) was added. Briefly, the alamarBlue® reagent was mixed 1:10 with fresh DMEM/10%FBS followed by a 1.5 h incubation at 37°C. For co-culture system, cells in insert and bottom chambers were incubated 1.5 h separately in alamarBlue/DMEM/10%FBS mixture (e. g., inserts were moved into fresh well plate). Results were evaluated by monitoring fluorescence at excitation wavelengths of 530 nm with emission at 590 nm using top reading mode (Synergy HT, BioTek, USA). The top reading mode prevented the signal collection from adherent cells, which minimized interference from intracellular NP. Cell viability was calculated using the expression (fluorescence intensity (FI) of test sample- FI of reagent blank)/(FI of untreated control-FI of reagent blank) × 100.

2.6 | Cell death process of N2a

Cell death process was evaluated for direct and indirect effects of AgNPs on differentiated N2a cells. For direct exposure, N2a cells (5×10^3 cells cm^{-2}) were seeded in six-well culture plates. For indirect exposure, the coculture system of ALT-N2a and BV-2-N2a were prepared based on above mentioned procedures. Live, necrotic, and apoptotic cells were distinguished using an Annexin V-FITC/propidium iodide (PI) assay kit (biotool.com, Houston, TX). Sample preparation was conducted according to the manufacturer's protocol. Fluorescence channel FITC and PerCP-Cy5.5 were used to detect Annexin V and PI in BD FACSCanto II flow cytometer (BD Biosciences, San Jose, CA), with 10,000 cells collected. Data was analyzed using Flowing Software 2.

2.7 | NP uptake potential and quantification

Uptake potential of AgNPs was measured by flow cytometry light-scatter analysis developed by Suzuki et al.[33] After 24 h of NP exposure, suspensions were removed, and the cells were rinsed three times with phosphate-buffered saline (PBS). Next, the cells were harvested and washed gently once with PBS. Evaluation of geometric mean side scatter (SSC) intensity was carried out using a FACSCanto II, and data were analyzed using Flowing Software 2. Data was calculated using the expression (SSC intensity of test sample)/(SSC intensity of untreated control or LPS-only treated control) × 100.

Laser ablation-ICP-MS (Laser ablation system: New Wave Research, ESI, USA; ICP-MS: Agilent 7500a, USA) was used to realistically quantify uptake of AgNPs in single cell. Details of the sample preparation and measurements had been presented in our previous study.[29]

2.8 | Intracellular ROS

Production of H_2O_2, a major intracellular ROS, was measured using 2′,7′-dichlorofluorescin diacetate (DCFH-DA, Sigma–Aldrich, MO) as a reactive fluorescent probe. The intracellular ROS and uptake potential could be measured simultaneously.[34] The DCFH-DA working solution (10 μM) in serum and phenol red-free DMEM, was added to each collected cell, followed by incubation for 30 min at 37°C. The solution was then centrifuged (200 g, 5 min) and the supernatant was removed. Prior to measurement, the cells were re-suspended in PBS. Then, 2 mM of H_2O_2 were treated for 15 min before the end of NP exposure as a positive control. Fluorescence was determined at 528 nm after excitation at 488 nm laser (FITC channel) using a FACSCanto II flow cytometer, with 10,000 cells collected. Data was analyzed using Flowing Software 2. About 50% of total cells that had higher fluorescence intensity in control sample were gated by histogram analysis. Any increased or decreased distribution of fluorescence intensity from other samples would get a higher or lower percentage of cells within gating range.

2.9 | Extracellular NO and H_2O_2

Cells (1×10^4 cells cm^{-2} for ALT and BV-2) were first seeded in 24-well plates. After 4 and 24 h AgNP exposure, the 0.5 mL suspensions were collected. To avoid interference, most of the serum in suspensions was removed using 10 kDa molecular weight cut-off filters (Pall, NY) with 14,000*g* centrifugal force at 4°C. Then, aliquot of samples (20 μL for Nitrite assay; 5 μL for H_2O_2 assay) were used based on the manufacturer's protocols (Nitrate/Nitrite fluorometric assay kit [Cayman Chemical Company, MI; Hydrogen peroxide fluorescent detection kit (Arbor Assays, MI)]. After performing the assays, results were evaluated by monitoring fluorescence at an excitation wavelength of 360 nm

with emission at 430 nm for nitrite assay and an excitation wavelength of 560 nm with emission at 590 nm for hydrogen peroxide assay.

2.10 | Chemokine/Cytokine Detection

Supernatants, which were collected from well plate (monoculture) or from bottom and upper Transwell chambers (coculture), were used for cytokine measurement. They were stored in −80°C until used. Pro-inflammatory mediators IL-6, TNF-α, and MCP-1 were measured by a commercially available ELISA Development Kit (eBioscience, CA) according to the manufacturer's protocol. To test whether AgNPs in medium disturbed detection of cytokines, standard IL-6 (250 pg mL^{-1}), TNF-α (500 pg mL^{-1}), and MCP-1 (1200 pg mL^{-1}) were added to the AgNP suspensions (3 μg mL^{-1} in DMEM/10% FBS), respectively. A 100 μL of each sample was used for triplicate ELISA analysis. Supporting Information Figure S1 showed that no any interferences of AgNP on the cytokine detection by ELISA.

2.11 | Uptake mechanisms

The energy-dependent uptake mechanism experiment was conducted by pre-incubating ALT or BV-2 cells at 4 or 37°C for 30 min prior to 2 h of AgNPs exposure (3 μg mL^{-1}). For endocytic pathway inhibition experiments, ALT, BV-2, and LPS-activated BV-2 cells were preincubated for 30 min with different inhibitors at the following concentrations: genistein (100 μM), filipin III (1.5 μM for ALT; 7.5 μM for BV-2), amiloride hydrochloride (100 μM), chlorpromazine hydrochloride (CPZ) (14 μM), monodansylcadaverine (MDC) (75 μM) and phenylarsine oxide (PAO) (0.006 μM for ALT; 0.3 μM for BV-2) (all from Sigma–Aldrich, St. Louis, MO). Mechanism of action of pharmacological inhibitors was shown in Supporting Information Table S1. After pre-incubation, AgNPs (3 μg mL^{-1}) were added and incubated for 2 h. To study Ca^{2+}-regulated clathrin- and caveolae-independent endocytosis in astrocyte-like cells, ALT was pre-incubated for 45 min with Ca^{2+} chelator BAPTA-AM (25 μM) (TCI, Tokyo, Japan). AgNPs were then added and incubated for 1.5 h. After exposure, the suspensions were discarded and cells were washed once with PBS. A mixture of 10 mM tripotassium hexacyanoferrate (III) ($K_3Fe(CN)_6$) and 10 mM sodium thiosulfate pentahydrate ($Na_2S_2O_3{\cdot}5H_2O$) (both from Sigma–Aldrich, St. Louis, MO) in PBS (PBS-Fe^{3+}-$S_2O_3{}^{2-}$) was then added to each well for 30 s to remove membrane-bound particles.[35] Finally, cells were washed again with PBS, trypsinized and harvested. To count the cell concentration, 10 μL of suspension was taken from harvested cells. After centrifugation (250 g, 5 min), supernatant was discarded and the cell pellet was acidified with 1 mL 65% HNO_3. Suspensions were then digested at 70°C for 24 h and filled to 15 mL with 10 ppb of Rh as internal standard before analysis. ^{107}Ag and ^{103}Rh analysis was conducted using a quadrupole ICP-MS (Agilent 7500a, USA). Prior to the experiment, we had analyzed the cytotoxicity of the inhibitors after 2.5 h by alamarBlue® and used only subcytotoxic doses (cell viability higher than 80%)(data not shown). BODIPY-LacCer (lactosylceramide complexed to BSA, 0.5 μM) (for Genistein and Filipin), Transferrin-Alexa Fluor 488 (0.25 μg mL^{-1}) (for CPZ and MDC) and Dextran-Oregon Green 488; 70,000 MW (12 μg mL^{-1}) (for Amiloride and PAO) (all from Life Technologies, CA) were used as control substrates to measure the efficiency of inhibitors. The inhibitors were pre-incubated for 30 min, and then the substrate was added and incubated for 2 h. Fluorescence was determined at 528 nm after excitation at 488 nm using a FACSCanto II flow cytometer, with 10,000 cells collected.

2.12 | Lysosome tracking

Cells were treated with AgNP (3 μg mL^{-1}) suspensions for 5, 8, 16, and 24 h after seeding 5.2 × 10^3 cells cm^{-2} on coverslips in 12-well culture plates. After incubation, 500 nM LysoTracker Green DND-26 (Life Technologies, CA) was added and incubated at 37°C for 10 min (for ALT) or 20 min (for BV-2 and LPS-activated BV-2). Cells were washed with PBS-Fe^{3+}-$S_2O_3^{2-}$ as uptake mechanism experiment. Cells were then fixed with 4% paraformaldehyde (PFA) in PBS for 20 min at room temperature. Coverslips were covered by ProLong® antifade mountant with DAPI (Life Technologies, CA) for nuclei staining. Images were obtained from the combination of fluorescence and dark field microscopy with 60× Plan Fluor with an iris diaphragm (Nikon Ti-U series microscopy, Japan), or confocal laser scanning microscopy (CLSM) system (LSM 780, Carl Zeiss, Göttingen, Germany) with a 63× oil-immersion objective using 561 nm laser excitation for imaging AgNPs in reflectance mode, 405 nm laser for DAPI, and 488 nm laser for LysoTracker Green.

2.13 | Quantifying AgNPs in cells after direct or indirect exposure

Cells (5 × 10^3 cells/cm^2 for N2a; 1 × 10^4 cells/cm^2 for BV-2) were seeded in the insert of six-well Transwell® plates (indirect exposure) or six-well plates (direct exposure). After attachment and differentiation, cells were incubated in serum-free medium for 6 h. Then, a final concentration of AgNPs (3 μg mL^{-1}) was added in the lower chamber of Transwell plates or culture plates and incubated for 24 h. The NP suspensions were then discarded and cells were washed with PBS-Fe^{3+}-$S_2O_3^{2-}$ as uptake mechanism experiment. Procedures for ICP-MS quantification of NPs in cells were the same as in the uptake mechanisms study.

2.14 | Statistics

Significant differences between control/LPS-only group and treatment groups were analyzed in GraphPad Prism (version 5.02) by one-way analysis of variance (ANOVA) followed by Dunnett's multiple comparison post-tests. For two-group comparison, Student's unpaired *t* test was used. $P < 0.05$ was considered statistically significant.

3 | RESULTS

3.1 | NP physicochemical characterization

Characteristics of AgNPs (primary, hydrodynamic size, size distribution, surface charge, stability, and dissolution in medium) were discussed in

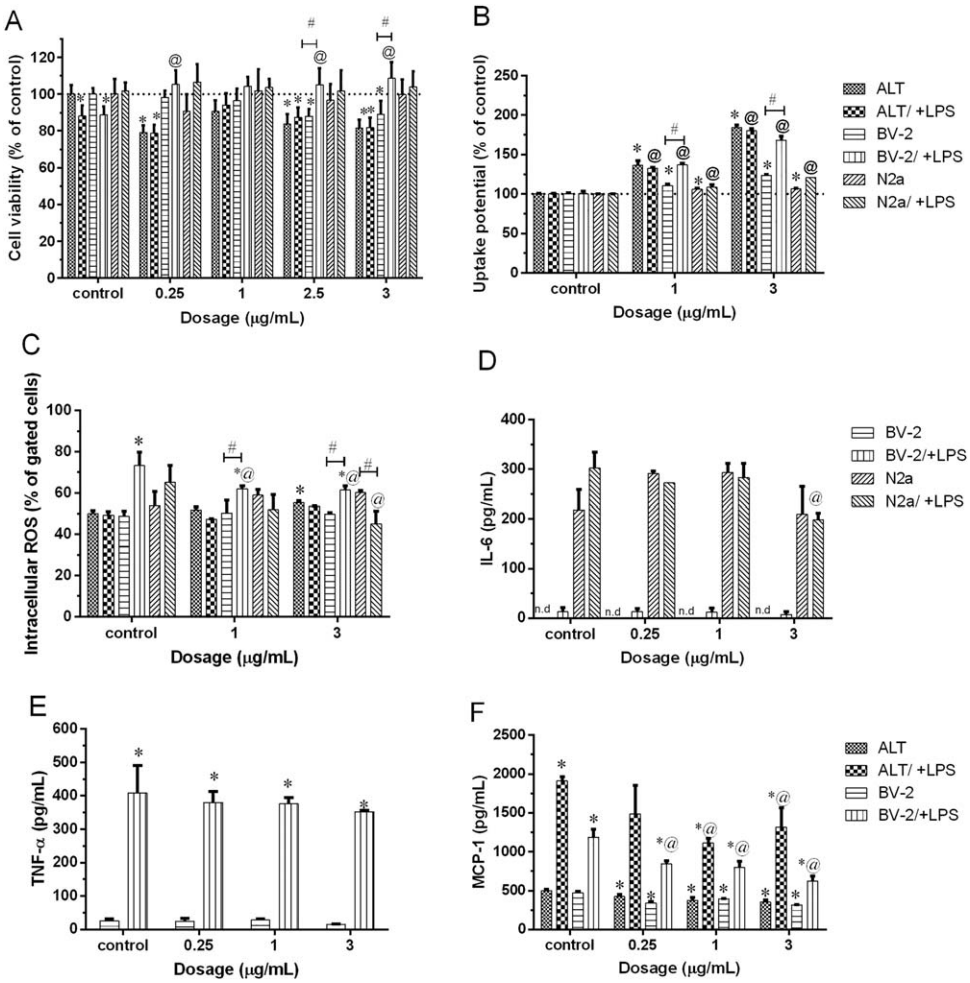

FIGURE 1 Direct effects of AgNPs with (+) or without LPS co-treatment in ALT, BV-2 and differentiated N2a cells after 24 h. (A) cell viability; (B) uptake potential; (C) intracellular ROS; (D) IL-6 release; (E) TNF-α release; (F)MCP-1 release. Data are presented as means ± SD (for cell viability $n = 4$; for others $n = 3$). (*) Significantly different from the control group. (@) Significantly different from the LPS-only treatment group. (#) Significantly different between two treatment groups

the Supporting Information. Briefly, geometric mean size of AgNPs was 9.7 nm, with uniform spheres (Supporting Information Figure S2). Dynamic laser scattering (DLS) measurement showed that AgNPs was 53 nm in culture medium, and had good stability within 48 h (Supporting Information Table S2 and Figure S3). However, the initial DLS sizes of AgNPs decreased with the decrement of concentration (Supporting Information Figure S3), which could be explained by different ratios between AgNPs and DMEM/10%FBS medium (Supporting Information Figure S4). When 1, 2.5, and 3 μg mL^{-1} of AgNPs was added into cell medium, 90%, 40%, 53% of AgNPs were dissolved into Ag ions at 24 h, respectively (Supporting Information Figure S5).

3.2 | Direct effects: Cytotoxicity of AgNPs

Figure 1A and Supporting Information S6 show the cell viability of ALT, BV2, and differentiated N2a cells for 24 and 48 h, respectively. AgNPs had a dose-, time-, and cell type-dependent toxicity. They caused the most pronounced cytotoxicity on ALT, following BV-2, and the least on differentiated N2a. No cytotoxicity was presented at 24 h in N2a, but only at 48 h. Uptake potential was then analyzed by flow cytometry after 24-h exposure. The uptake profiles were clearly dose- and cell dependent (Figure 1B). ALT took up the highest amount of AgNPs, followed by BV-2, with the lowest in N2a. Our previous study also supports the results in this study, which used LA-ICP-MS to quantify the AgNP uptake in single cell level (Supporting Information Figure S7). The cell viability correlated well with the uptake level in the three cell types. The intracellular ROS of three cell lines were measured using the DCFH-DA assay. ROS was significantly induced in ALT at 3 μg mL^{-1}, while was not induced in BV-2 and N2a after 4 and 24 h (Supporting Information Figure S8and Figure 1C). IL-6, TNF-α, and MCP-1 were selected as inflammation markers because these mediators play a major role in prevention, and also enhance brain damage. These cytokines also participate in the inflammation process of neurodegenerative disorder (e. g., Alzheimer's disease).[36] In this study, AgNPs neither induced IL-6 and TNF-α in BV-2 (IL-6 and TNF-α) nor in N2a cells (IL-6) (Supporting Information Figure 1D,E). MCP-1 was even inhibited in ALT and BV-2 cells (Figure 1F).

Treatment of LPS caused mild toxicity in ALT and BV-2 cells (70–90% of cell viability), while not showing toxicity in N2a (Figure 1A).

After co-treatment of AgNPs with LPS for 24 and 48 h, the cell viabilities were similar to NP-only treatment groups on ALT and N2a. Compared with the LPS-only group, significant increase of cell viability was found in BV-2 when co-treated with LPS and AgNPs (0.25, 2.5, and 3 μg mL^{-1}) (Figure 1A). On the other hand, LPS-activated BV-2 cells took up larger amounts of AgNPs than normal BV-2 cells, while there were no differences in NP uptake between normal and LPS-treated ALT and N2a cells (Figure 1B). LPS induced intracellular ROS release in BV-2 after 24 h, while the induction was inhibited after co-treating with AgNPs (Figure 1C). Similar results could be found in 4 h data (Supporting Information Figure S8). LPS induced IL-6 in BV-2 and N2a, TNF-α in BV-2 and MCP-1 release in ALT and BV-2. However, the induction was inhibited after co-treated with AgNPs in N2a (IL-6), ALT and BV-2 (MCP-1) (Figure 1D, F). All three cytokines were significantly inhibited in the activated BV-2 after 48 h of exposure, which correlated well with abovementioned ROS release results (Supporting Information Figure S9).

3.3 | Direct effects: Cell death process of differentiated N2a

The cell death mechanisms (necrosis/apoptosis) of neurons were measured because the apoptosis cascades involved in Alzheimer's disease and other human neurological disorders.[37] The cell death process of N2a cells after direct AgNP exposure for 24 h was detected by Annexin V/PI staining. The results are shown in Figure 2. The AgNPs induced apoptosis (12.9%) in differentiated N2a cells and also as they were cotreated with LPS (11.2%) at 3 μg mL^{-1}. More apoptotic (14.4%) and necrotic cells (9.3%) were observed at 6 μg mL^{-1}. No significant difference was observed between LPS-only and control groups.

3.4 | Direct effects: Uptake mechanisms and lysosome tracking in ALT and BV-2

Because of NPs being mainly taken up by astrocyte-like cells, microglia and LPS-activated microglia, we studied the mechanisms of NP uptake in those cells. This could be helpful to realize the portion and velocity at which NPs can enter into lysosome, an important place to trigger ROS. To determine major uptake pathways of AgNPs, we first considered whether the uptake was a passive process. Cell cultures were incubated at 37°C or at 4°C to block several proteins and enzymes which are needed for active processes. Exposure to AgNPs at 4°C resulted in a very strong inhibition of endocytosis of both ALT and BV-2 (Supporting Information Figure S10), which indicated that the uptake in both cells were an active process. Then, general active uptake mechanisms, including clathrin-dependent, caveolae-dependent endocytosis, macropinocytosis and phagocytosis were considered. Inhibitors genistein, filipin (for caveoleo-dependent), chlorpromazine, MDC (for clathrin-dependent), amiloride (for macropinocytosis) and PAO (for phagocytosis/clathrin-dependent endocytosis) were used. We analyzed the efficiency of these inhibitors in our cell systems by using transferrin (clathrin-dependent), lactosylceramide (LacCer) (caveoleo-dependent) and dextran-70000MW (for the other two pathways) as substrates.[38,39] Filipin, amiloride, and PAO all showed inhibited effects on

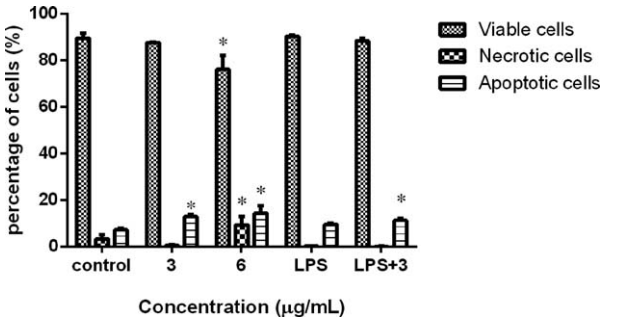

FIGURE 2 Effect of AgNPs on the cell death process of N2a. The percentage of viable, necrotic and apoptotic cells after being exposed to 3 or 6 μg mL^{-1} AgNPs for 24 h. Data are presented as means ± SD ($n = 3$). (*) Significantly different from the control group

the uptake of their corresponding substrates to the three cells (Supporting Information Figure S11). Genistein did not inhibit the uptake of LacCer in BV-2 (Supporting Information Figure S11B). Chlorpromazine and MDC could inhibit the uptake of transferrin in BV-2, but not in ALT and activated BV-2 cells (Supporting Information Figure S11). The inhibitors may impair the cells in their morphology and activate other endocytic pathways to take up transferrin even though they did not decrease the cell viability within 2.5 h.[40] Previous study also has confirmed a lack of specific positive controls for distinct endocytic pathways.[41] Figure 3 shows analysis of uptake mechanisms of AgNPs using different inhibitors. Only PAO slightly decreased the uptake of AgNPs in ALT, which inhibited phagocytosis/clathrin-mediated endocytosis (Figure 3A). Moreover, amiloride, CPZ, MDC, and PAO all inhibited the uptake of AgNPs in BV-2, which inhibited macropinocytosis, clathrin-dependent, and phagocytosis pathways (Figure 3B). All inhibitors decreased the uptake of AgNPs in LPS-activated BV-2, except genistein, which means all pathways we considered were involved (Figure 3C). Finally, Ca^{2+}-regulated clathrin- and caveolae-independent endocytosis, which was found specifically in astrocytes,[42] was considered. Because this endocytosis can be tightly regulated by intracellular Ca^{2+}, Ca^{2+} chelator BAPTA-AM was used as inhibitor for uptake mechanism study. The results found uptake of AgNPs significantly decreased when using the inhibitor, which demonstrated that AgNPs were partially involved in the indicated pathways in ALT (Figure 3).

Whether or not AgNPs translocate into lysosome relates to its toxicity. One reason is that NPs may induce ROS from lysosome, which is one of major source of cellular ROS release.[43] The other is that the acidic environment of the lysosomes may trigger the release of relatively toxic ions (e. g., Ag^{+}, Cd^{2+}, $Fe^{2+/3+}$ ions) from NPs.[44] To elucidate intracellular tracking of NPs, we investigated co-localization of internalized AgNPs with Lysotracker Green which stains acidic compartments, such as late endosomes and lysosomes. To view NPs, we used dark-field microscopy and reflectance mode confocal microscopy.[45–47] We found partial colocalization of AgNPs and lysosome from 5 to 24 h of exposure in ALT cells, from 16 to 24 h in BV-2, and from 8 to 24 h in LPS-activated BV-2 (Figure 4). Thus, AgNPs could enter into lysosomes with different velocity for three cells.

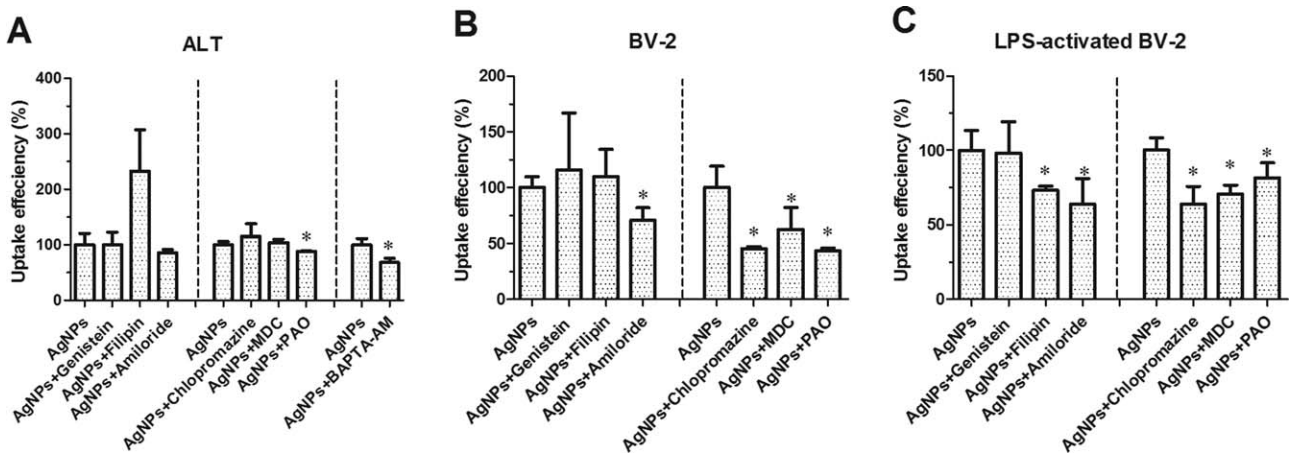

FIGURE 3 Analysis of uptake mechanisms of AgNPs different inhibitors. Cells were pretreated with various inhibitors (Genistein, Filipin, Chlorpromazine, MDC, Amiloride and PAO) for 30 min, followed by exposure to AgNPs in ALT, BV-2 and LPS-activated BV2 for 2 h. Ca^{2+} chelator BAPTA-AM (25 μM; 45 min) was pretreated to decrease intracellular Ca^{2+} in ALT, followed by exposure to AgNPs for 1.5 h. The data was measured by ICP-MS with normalization of cell number. Data are presented as means ± SD ($n = 3$). (*) Significantly different from the control group (AgNPs treatment without inhibitors)

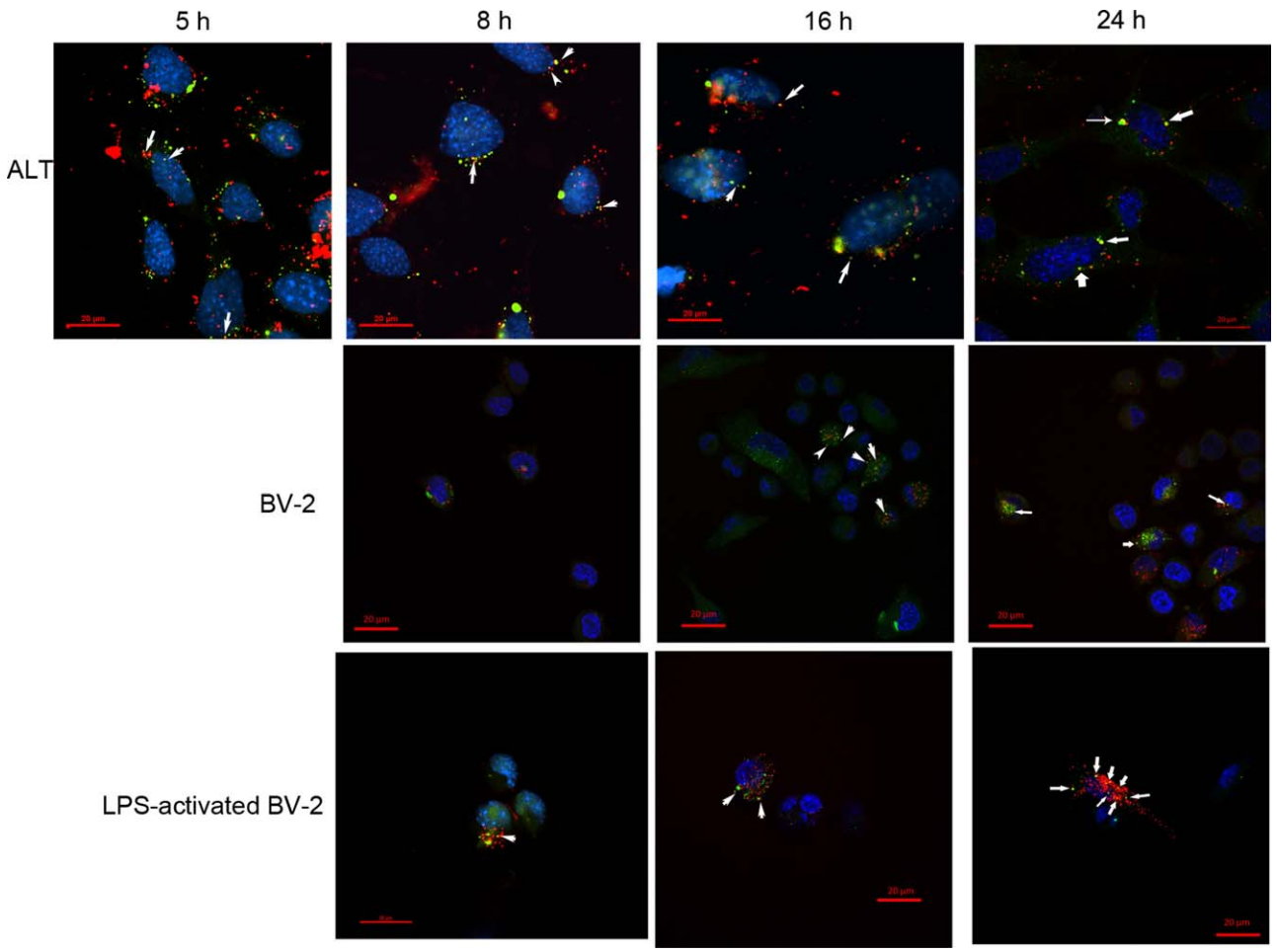

FIGURE 4 Colocalization of AgNPs and lysosomes in ALT, BV2 and LPS-activated BV-2 after 5, 8, 16, and 24 h of exposure. NPs are depicted in red, lysosomes are stained in green using Lysotracker Green and nuclei are depicted in blue using DAPI. Co-localization of NPs and lysosomes is indicated by yellow color in the merged image resulting from overlaying green and red color. White arrows indicate the spots of yellow color. ALT images were derived from dark field coupled with fluorescence microscopy. Others images were derived from reflectance mode of confocal laser scanning microscopy. Scale bar = 20 μm [Color figure can be viewed at wileyonlinelibrary.com]

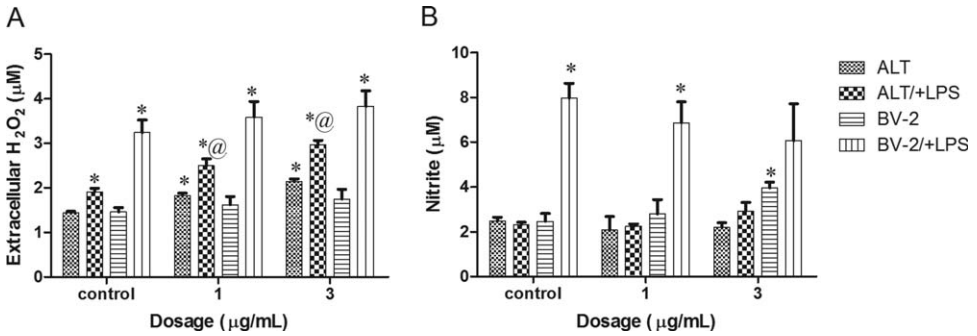

FIGURE 5 Extracellular release of (A) H_2O_2 and (B) NO from ALT and BV-2 after treatment with 1 or 3 μg mL^{-1} AgNPs with (+) or without LPS cotreatment for 24 h. Data are presented as means ± SD ($n = 3$). (*) Significantly different from the control group. (@) Significantly different from the LPS-only treatment group

3.5 | Direct effects: Extracellular H_2O_2 and NO production from ALT and BV-2

Here, extracellular H_2O_2 and NO released from BV-2 and ALT were measured. After 4 h, LPS-activated BV-2 released significant H_2O_2 into medium, while co-treatment of AgNPs decreased the release (Supporting Information Figure S12). After 24 h, extracellular H_2O_2 was significantly released from ALT by AgNPs. H_2O_2 was induced from each LPS-activated cell line. AgNPs induced more H_2O_2 from LPS-activated ALT (Figure 5A). AgNPs also induced significant NO from BV-2 after 24 h (Figure 5B). LPS-activated BV-2 induced NO release, but co-treatment of AgNPs did not enhance the release (Figure 5B). The results suggest that AgNPs might induce extracellular H_2O_2 release from ALT or NO from BV-2, and indirectly damaged N2a cells.

3.6 | Indirect effects: Cytotoxicity of AgNPs to N2a in ALT-N2a and BV-2-N2a coculture

To verify the abovementioned hypothesis, a coculture study between ALT/BV-2 and N2a was conducted using Transwell system. In general, three kinds of coculture systems were used frequently: (1) a conditioned medium transfer system (2) a direct co-culture system allowing cell-cell contact and communication and (3) a Transwell system, which allows communication through diffusible and soluble factors with no cell contact.[48] We selected the Transwell system not only because it allows of cell-cell simultaneous interaction, thus avoiding loss of short half-life species such as ROS when using conditioned medium transfer system, but it also distinguishes the responses occurring in different kinds of cells after AgNP exposure. The system also can neglect the contribution of cell-cell contact (such as disruption of CD200/CD200r between neurons and microglia[49]) on indirect effects of NPs. To demonstrate the indirect AgNP effects on N2a cells, it is essential to prove significantly less amount of AgNPs in the N2a cells of Transwell insert than that in well plate. We thus compared the amount of AgNPs in N2a cell between direct and indirect exposure at the same dosage by ICP-MS (Supporting Information Figure S13A). The indirect exposure showed in a 65% of Ag compared with direct exposure in N2a (Supporting Information Figure S13B). This indicated that if there were more harmful effects on N2a from coculture study, stimulants triggering from indirect NP exposure should be considered. Indirect exposure of 6 μg mL^{-1} AgNPs and 3 μg mL^{-1} AgNPs with LPS induced more apoptotic N2a cells (27.3 and 22.1%, respectively) in ALT-N2a co-culture than their direct effect on N2a (Figure 6A,C). Corresponding to the cell death process, viability of N2a decreased significantly to 90 and 86% when the AgNPs cotreated with LPS to ALT at 1 and 3 μg mL^{-1} (Supporting Information Figure S14A). However, the intracellular ROS was inhibited in N2a cells for both AgNP and AgNP-LPS cotreatment groups (Supporting Information Figure S14C). IL-6 and MCP-1 release in N2a supernatant (insert) were also inhibited for both AgNP and AgNP-LPS co-treatment groups (Supporting Information Figure S14E,G). On the other hand, more apoptotic N2a cells was observed in BV-2-N2a coculture after indirect AgNP exposure (14 and 21% for 3 and 6 μg mL^{-1}) (Figure 6B,D). Treatment of LPS in BV-2-N2a coculture increased apoptotic N2a, while no further increased apoptosis rate was observed when co-treated AgNPs (Figure 6D). Neither AgNPs nor AgNPs-LPS cotreatment induced more ROS released in BV-2 and N2a (Supporting Information Figure S13D). Indirect AgNP exposure inhibited the MCP-1 release in N2a-containing chamber, while the decrease of MCP-1 release after AgNP-LPS cotreatment was observed in BV-2 (Supporting Information Figure S14H). Neither AgNPs nor AgNPs-LPS cotreatment induced more IL-6 and TNF-α released (Supporting Information Figure S14F and S15).

3.7 | Indirect effects: Cytotoxicity of AgNPs to BV-2 in ALT-BV-2 coculture

In addition to indirect effects of AgNPs on N2a, we also investigated their indirect effects on BV-2 cells in a coculture of ALT and BV-2 cells. The amounts of Ag in each BV-2 cell for direct and indirect exposure was compared (Supporting Information Figure S13). The indirect exposure showed only a 22% of Ag compared to direct exposure in BV-2 (Supporting Information Figure S13B). The viability of BV-2 decreased significantly to 86% as indirect AgNP exposure and was significantly lower in LPS co-treatment group (74%) at 3 μg mL^{-1} (Figure 7B). Corresponding to the cell viability results, the intracellular ROS was induced in BV-2 when the indirect treatment of AgNPs or AgNP-LPS (Figure 7C). However, indirect AgNP and AgNP-LPS treatment did not

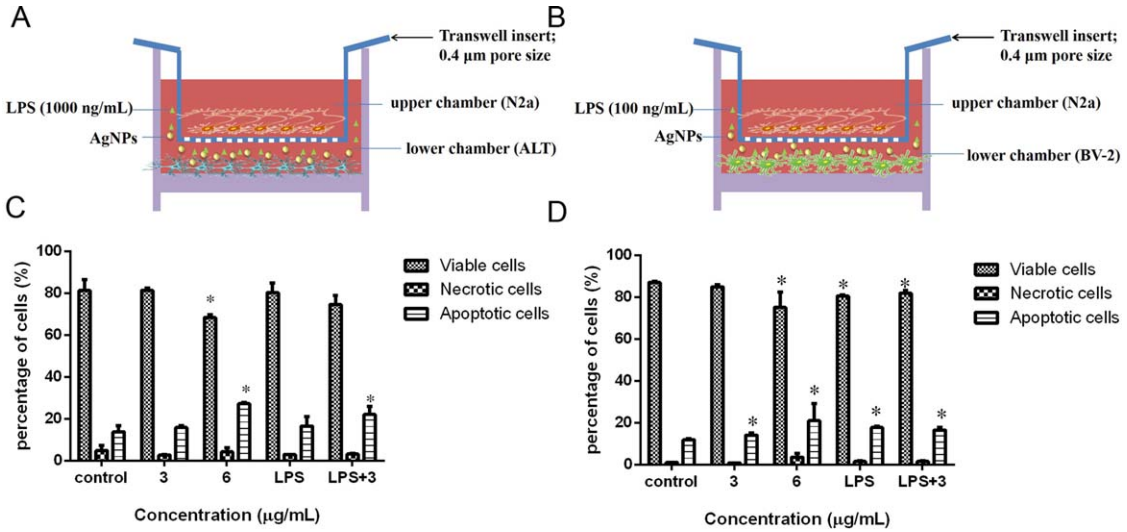

FIGURE 6 Effect of indirect AgNPs exposure on the cell death process of N2a. (A): ALT-N2a coculture; (B) BV-2-N2a coculture. (C)(D) The corresponding percentage of viable, necrotic and apoptotic after being exposed to 3 or 6 μg mL^{-1} AgNPs for 24 h. Data are presented as means ± SD ($n = 3$). (*) Significantly different from the control group [Color figure can be viewed at wileyonlinelibrary.com]

induce further more IL-6, TNF-α and MCP-1 from both chambers (Supporting Information Figure S16).

4 | DISCUSSION

4.1 | Astrocytes and microglia are more susceptible to AgNPs than neurons

In our study, 10 nm AgNPs caused the highest cytotoxicity on astrocyte-like cells, followed by microglia, and the least on neuron-like cells, which correlated well with NP uptake. Similar to our study, magnetic NPs in primary neural cell cultures were mainly taken up by microglia, followed by astroglia, oligodendroglia and neurons.[50] In mixed primary cell models (containing neurons and astrocytes), Haase et al. found that astrocytes were much more vulnerable to 20 nm peptide-coated AgNPs compared with neurons, and also in consistent with cell uptake capability.[22] Generation of ROS and induction of heme oxygenase-1 also have been found in mixed primary cortical cell in the same report. Sun et al. found that PVP-coated AgNPs induced ROS in a time and dose-dependent manners in rat cerebral astrocytes.[21] Our study further found that the ROS was mainly generated by astrocytes.

4.2 | Activated microglia take up large amounts of AgNPs, while do not cause more toxicity

Most reports discussed the uptake and toxicity of activated microglia on magnetic NPs because they have wide application as magnetic resonance imaging contrast agents.[51,52] One report indicated that LPS-

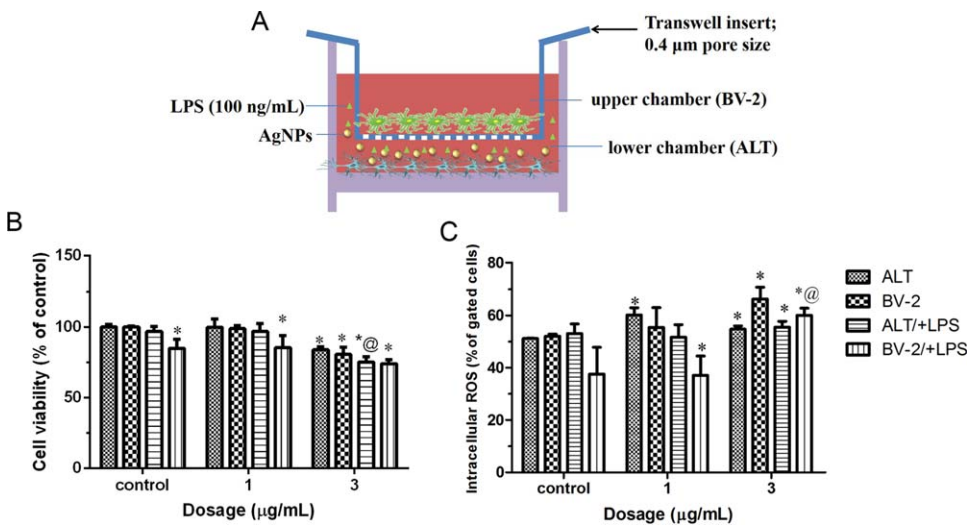

FIGURE 7 Effects of AgNPs in ALT-BV-2 coculture system. (A) illustration of indirect AgNP exposure in ALT-BV-2 coculture. (B) Cell viability; (C) intracellular ROS after treatment of AgNPs for 24 h. Data are presented as means ± SD ($n = 3$). (*) Significantly different from the control group. (@) Significantly different from the only LPS treatment group [Color figure can be viewed at wileyonlinelibrary.com]

mediated stimulation of magnetic NP uptake was transient, and might be more related to early steps in the activation process.[23] Our study found that LPS-activated BV-2 were induced to take up more AgNPs when pretreated with LPS for short times (6 h) followed by NPs exposure for 24 h, which supports the suggestion. Besides, treatment of AgNPs to LPS-activated BV-2 decreased the cytotoxicity of LPS. This might be explained by the AgNP-inhibited ROS production. The large amount of uptake of AgNPs, which has a high capability to react with H_2O_2 in LPS-activated BV-2, inhibits the ROS.[29]

4.3 | AgNPs cannot induce and even inhibit cytokine release from cells

Few reports concerned about AgNP-induced inflammation responses in brain cells. AgNPs induced TNF-α, IL-1β, PGE2 in primary rat brain microvessel endothelial cells, which are outside layer of BBB.[53] Secretion of CINC-2α/β, CINC-3, fratalkine, IL-10, IP-10, L-selectin, and thymus chemokine were observed in AgNP-exposed rat astrocytes.[21] Our previous study found that AgNPs upregulated CXCL13 and MARCO genes in ALT, BV-2 and N2a, which are immune mediators in response to inflammation.[54] Transcription factor NF-κB activity is regulated by intracellular ROS, which then mediates release of proinflammatory cytokines (MCP-1, TNF-α, IL-6).[55] The inhibition of cytokines release correlated well with ROS production in three activated brain cells, which indicates ROS is a major factor in mediating those inflammation markers. To further confirm the neuro-inflammation, others cytokines and chemokines should be analyzed for future study. Interestingly, the inhibition of IL-6 or MCP-1 was found in our mono- and co-culture study. Low amounts of IL-6 enhance the differentiation and survival of neuronal cell lines and primary neurons.[56] MCP-1, one of chemokines serves to regulating microglial movement, protects human neurons and astrocytes damage against different stimuli. Thus, inhibition of IL-6 and MCP-1 may decrease the survival of neuron-like cells, neuron differentiation and microglia clearance function.

4.4 | Uptake mechanism of AgNPs is cell type dependent, which causes different NP translocation rates into lysosomes

In brain, phagocytosis occurs mainly in microglia and increases in activated state. Astrocytes also could undergo phagocytosis to a lesser extent than microglia.[57] This may explain phagocytosis found in the uptake of AgNPs in ALT to a lesser degree or not at all compared to BV-2. Our study found that LPS-activated microglia was involved in more uptake mechanisms for engulfing AgNPs than normal microglia and astrocyte-like cells. This can be expected, because the activated microglia acts with macrophage-like functions. Besides, uptake mechanisms were different between ALT, BV-2 and LPS-activated BV-2. This demonstrates cell type-dependent uptake mechanisms.

Uptake mechanisms of NPs would determine whether they could be translocated into lysosome, as well as how fast they were translocated. In phagocytosis, formation of phagosome vesicles will fuse with lysosomes within a few minutes.[58] The transportation rate of nutrients from early endosomes to lysosomes by Ca^{2+}-regulated clathrin-, caveolae-, and dynamin-independent endocytosis takes place within 15 min.[42] The translocation of NPs into lysosome via the pathway of clathrin-mediated endocytosis primarily needs a few hours. Particles which are taken up by macropinocytosis form macropinosomes and fuse with lysosomes generally more slowly than clathrin-mediated pathways.[59] Caveolae-mediated endocytosis was the only pathway in this study that could bypass lysosomes. Therefore, we could expect that (1) AgNPs can finally enter into lysosomes of ALT, BV-2 and LPS-activated BV-2, because at least one lysosome-related uptake mechanism was involved. (2) AgNPs would be transported to lysosome more rapidly in ALT cells than in BV-2 due to involvement of Ca^{2+}-regulated clathrin-, caveolae-independent endocytosis. Corresponding to our expectation, we found partial co-localization of AgNPs and lysosome in the three cells, and the translocation rate is the fastest in ALT. Reasons for the partial colocalization of AgNPs and lysosomes include (1) some AgNPs that be taken up via macropinocytosis in microglia or LPS-activated microglia still do not enter into lysosome after 24 h. (2) some AgNPs in lysosomes are dissolved by the acidic surroundings, or (3) AgNP oxidation with ROS.

4.5 | AgNPs can damage N2a cells indirectly by NO release from BV-2 or H_2O_2 from ALT cells

AgNPs directly induced apoptosis and necrosis in N2a cells. However, more apoptotic but no necrotic N2a was induced after indirect treatment of AgNPs or cotreatment of AgNPs with LPS to ALT. This may be explained by high H_2O_2 release from ALT because previous studies have found that H_2O_2-induced apoptosis in neuron cells.[60] In addition, high level of H_2O_2 in medium would increase AgNP oxidative dissolution rate and release more toxic Ag ions, which also might be a reason to damage neurons.[29] The same reason could explain the decreased BV-2 viability in ALT-BV-2 coculture experiment.

The increased apoptotic N2a cells after indirect AgNPs exposure in BV-2-N2A coculture system may be attributed to the NO production which we found in mono-culture study. The NO damages neurons because it inhibits respiratory chain, rapids release of glutamate, and finally causes excitotoxic damage.[61,62] It is known that LPS can activate microglia, release soluble factors, such as IL-6, TNF-α, nitric oxide, and ROS and destroy neurons.[63] In this study, LPS treatment (1 μg mL^{-1}) to N2a did not lead to cell apoptosis (Figure 2B). However, a treatment of LPS (0.1 μg mL^{-1}) in BV-2-N2a co-culturing induced more apoptotic N2a cells, which could be attributed to the release of soluble factors (extracellular H_2O_2, NO, and TNF-α) from BV-2 and served as a good positive control in the BV-2-N2a coculture experiments.

5 | CONCLUSIONS

This study provides important insights into the toxic mechanism of AgNPs in CNS system. By direct NP exposure, AgNPs were mainly taken by ALT and BV-2 cells via different uptake mechanisms. Involvement of Ca^{2+}-regulated clathrin-, caveolae-independent endocytosis, and phagocytosis in ALT caused more rapid trafficking rates of AgNPs

to lysosome than in macropinocytosis and clathrin-dependent endocytosis-involved BV-2. By indirect AgNP exposure in Transwell system, relatively less NPs was detected in upper chamber cells than direct NP exposure to the same cells in well plate, which diminished effects from NPs. Indirect exposure of AgNPs caused not only apoptosis of N2a by NO release from BV-2, but also apoptosis (N2a) or cell viability decrease (BV-2) by H_2O_2 release from ALT cells. These results suggested that AgNPs' ability to induced ROS and NO from astrocytes or microglia is a key factor to determine neurotoxicity.

REFERENCES

[1] Reidy B, Haase A, Luch A, Dawson KA, Lynch I. Mechanisms of silver nanoparticle release, transformation and toxicity: a critical review of current knowledge and recommendations for future studies and applications. *Materials*. 2013;6(6):2295–2350.

[2] Larguinho M, Baptista PV. Gold and silver nanoparticles for clinical diagnostics—from genomics to proteomics. *J Proteom*. 2012;75(10):2811–2823.

[3] Wilkinson LJ, White RJ, Chipman JK. Silver and nanoparticles of silver in wound dressings: a review of efficacy and safety. *J Wound Care*. 2011;20(11):543–549.

[4] Genter MB, Newman NC, Shertzer HG, Ali SF, Bolon B. Distribution and systemic effects of intranasally administered 25 nm silver nanoparticles in adult mice. *Toxicol Pathol*. 2012;40(7):1004–1013.

[5] Loeschner K, Hadrup N, Qvortrup K, et al. Distribution of silver in rats following 28 days of repeated oral exposure to silver nanoparticles or silver acetate. *Part Fibre Toxicol*. 2011;8:18.

[6] Park EJ, Bae E, Yi J, et al. Repeated-dose toxicity and inflammatory responses in mice by oral administration of silver nanoparticles. *Environ Toxicol Pharmacol*. 2010;30(2):162–168.

[7] Tang JL, Xiong L, Wang S, et al. Distribution, translocation and accumulation of silver nanoparticles in rats. *J Nanosci Nanotechnol*. 2009;9(8):4924–4932.

[8] Ji JH, Jung JH, Kim SS, et al. Twenty-eight-day inhalation toxicity study of silver nanoparticles in Sprague-Dawley rats. *Inhal Toxicol*. 2007;19(10):857–871.

[9] Tang JL, Xiong L, Zhou GF, et al. Silver nanoparticles crossing through and distribution in the blood-brain barrier in vitro. *J Nanosci Nanotechnol*. 2010;10(10):6313–6317.

[10] Lee JH, Kim YS, Song KS, et al. Biopersistence of silver nanoparticles in tissues from Sprague–Dawley rats. *Part Fibre Toxicol*. 2013;10:36.

[11] Skalska J, Frontczak-Baniewicz M, Struzynska L. Synaptic degeneration in rat brain after prolonged oral exposure to silver nanoparticles. *Neurotoxicology*. 2015;46:145–154.

[12] Rahman MF, Wang J, Patterson TA, et al. Expression of genes related to oxidative stress in the mouse brain after exposure to silver-25 nanoparticles. *Toxicol Lett*. 2009;187(1):15–21.

[13] Wu J, Yu C, Tan Y, et al. Effects of prenatal exposure to silver nanoparticles on spatial cognition and hippocampal neurodevelopment in rats. *Environ Res*. 2015;138:67–73.

[14] Sofroniew MV, Vinters HV. Astrocytes: biology and pathology. *Acta Neuropathol*. 2010;119(1):7–35.

[15] Garden GA, Moller T. Microglia biology in health and disease. *J Neuroimmun Pharm*. 2006;1(2):127–137.

[16] Liu Z, Ren G, Zhang T, Yang Z. The inhibitory effects of nano-Ag on voltage-gated potassium currents of hippocampal CA1 neurons. *Environ Toxicol*. 2011;26(5):552–558.

[17] Powers CM, Badireddy AR, Ryde IT, Seidler FJ, Slotkin TA. Silver nanoparticles compromise neurodevelopment in PC12 Cells: critical contributions of silver ion, particle size, coating, and composition. *Environ Health Persp*. 2011;119(1):37–44.

[18] Tan JW, Ho CF, Ng YK, Ong WY. Docosahexaenoic acid and L-Carnitine prevent ATP loss in SH-SY5Y neuroblastoma cells after exposure to silver nanoparticles. *Environ Toxicol*. 2016;31(2):224–232.

[19] Luther EM, Koehler Y, Diendorf J, Epple M, Dringen R. Accumulation of silver nanoparticles by cultured primary brain astrocytes. *Nanotechnology*. 2011;22(37):375101.

[20] Luther EM, Schmidt MM, Diendorf J, Epple M, Dringen R. Upregulation of metallothioneins after exposure of cultured primary astrocytes to silver nanoparticles. *Neurochem Res*. 2012;37(8):1639–1648.

[21] Sun C, Yin N, Wen R, et al. Silver nanoparticles induced neurotoxicity through oxidative stress in rat cerebral astrocytes is distinct from the effects of silver ions. *Neurotoxicology*. 2016;52:210–221.

[22] Haase A, Rott S, Mantion A, et al. Effects of silver nanoparticles on primary mixed neural cell cultures: uptake, oxidative stress and acute calcium responses. *Toxicol Sci*. 2012;126(2):457–468.

[23] Pickard MR, Chari DM. Robust uptake of magnetic nanoparticles (MNPs) by central nervous system (CNS) microglia: implications for particle uptake in mixed neural cell populations. *Int J Mol Sci*. 2010;11(3):967–981.

[24] Long TC, Tajuba J, Sama P, et al. Nanosize titanium dioxide stimulates reactive oxygen species in brain microglia and damages neurons in vitro. *Environ Health Persp*. 2007;115(11):1631–1637.

[25] Xue Y, Wu J, Sun J. Four types of inorganic nanoparticles stimulate the inflammatory reaction in brain microglia and damage neurons in vitro. *Toxicol Lett*. 2012;214(2):91–98.

[26] Setyawati MI, Yuan X, Xie JP, Leong DT. The influence of lysosomal stability of silver nanomaterials on their toxicity to human cells. *Biomaterials*. 2014;35(25):6707–6715.

[27] Huang YH, Chen CY, Chen PJ, et al. Gas-injection of gold nanoparticles and anti-oxidants promotes diabetic wound healing. *Rsc Adv*. 2014;4(9):4656–4662.

[28] Yen HJ, Hsu SH, Tsai CL. Cytotoxicity and immunological response of gold and silver nanoparticles of different sizes. *Small*. 2009;5(13):1553–1561.

[29] Hsiao IL, Hsieh YK, Wang CF, Chen IC, Huang YJ. Trojan-horse mechanism in the cellular uptake of silver nanoparticles verified by direct intra- and extracellular silver speciation analysis. *Environ Sci Technol*. 2015;49(6):3813–3821.

[30] Leung YM, Huang CF, Chao CC, et al. Voltage-gated K+ channels play a role in cAMP-stimulated neuritogenesis in mouse neuroblastoma N2A cells. *J Cell Physiol*. 2011;226(4):1090–1098.

[31] Herculano-Houzel S. The glia/neuron ratio: how it varies uniformly across brain structures and species and what that means for brain physiology and evolution. *Glia*. 2014;62(9):1377–1391.

[32] Liu W, Tang Y, Feng J. Cross talk between activation of microglia and astrocytes in pathological conditions in the central nervous system. *Life Sci*. 2011;89(5/6):141–146.

[33] Suzuki H, Toyooka T, Ibuki Y. Simple and easy method to evaluate uptake potential of nanoparticles in mammalian cells using a flow cytometric light scatter analysis. *Environ Sci Technol*. 2007;41(8):3018–3024.

[34] Toduka Y, Toyooka T, Ibuki Y. Flow cytometric evaluation of nanoparticles using side-scattered light and reactive oxygen species-

mediated fluorescence-correlation with genotoxicity. *Environ Sci Technol*. 2012;46(14):7629–7636.

[35] Braun GB, Friman T, Pang HB, et al. Etchable plasmonic nanoparticle probes to image and quantify cellular internalization. *Nat Mater*. 2014;13(9):904–911.

[36] Rubio-Perez JM, Morillas-Ruiz JM. A review: inflammatory process in Alzheimer's disease, role of cytokines. *Sci World J*. 2012 (2012): 756357.

[37] Radi E, Formichi P, Battisti C, Federico A. Apoptosis and oxidative stress in neurodegenerative diseases. *J Alzheimers Dis*. 2014;42 (Suppl 3):S125–S152.

[38] Rejman J, Oberle V, Zuhorn IS, Hoekstra D. Size-dependent internalization of particles via the pathways of clathrin-and caveolae-mediated endocytosis. *Biochem J*. 2004;377:159–169.

[39] Zenni MK, Giardina PC, Harvey HA, et al. Macropinocytosis as a mechanism of entry into primary human urethral epithelial cells by Neisseria gonorrhoeae. *Infect Immun*. 2000;68(3):1696–1699.

[40] Andrei II. *Exocytosis and Endocytosis*. Springer; ISBN 978-1-59745-178-9, 2008, XV, 412 p.

[41] dos Santos T, Varela J, Lynch I, Salvati A, Dawson KA. Effects of transport inhibitors on the cellular uptake of carboxylated polystyrene nanoparticles in different cell lines. *Plos One*. 2011;6(9):e24438.

[42] Jiang M, Chen G. Ca^{2+} regulation of dynamin-independent endocytosis in cortical astrocytes. *J Neurosci*. 2009;29(25):8063–8074.

[43] Nohl H, Gille L. Lysosomal ROS formation. *Redox Rep*. 2005;10(4): 199–205.

[44] Sabella S, Carney RP, Brunetti V, et al. A general mechanism for intracellular toxicity of metal-containing nanoparticles. *Nanoscale*. 2014;6(12):7052–7061.

[45] Nitin N, Javier DJ, Roblyer DM, Richards-Kortum R. Widefield and high-resolution reflectance imaging of gold and silver nanospheres. *J Biomed Opt*. 2007;12(5):051505.

[46] Zucker RM, Daniel KM, Massaro EJ, Karafas SJ, Degn LL, Boyes WK. Detection of silver nanoparticles in cells by flow cytometry using light scatter and far-red fluorescence. *Cytometry A*. 2013;83(10):962–972.

[47] Zucker RM, Massaro EJ, Sanders KM, Degn LL, Boyes WK. Detection of TiO_2 nanoparticles in cells by flow cytometry. *Cytometry A 77A*. 2010;(7):677–685.

[48] Zujovic V, Taupin V. Use of cocultured cell systems to elucidate chemokine-dependent neuronal/microglial interactions: control of microglial activation. *Methods*. 2003;29(4):345–350.

[49] Walker DG, Lue LF. Understanding the neurobiology of CD200 and the CD200 receptor: a therapeutic target for controlling inflammation in human brains? *Future Neurol*. 2013;8(3).

[50] Pinkernelle J, Calatayud P, Goya GF, Fansa H, Keilhoff G. Magnetic nanoparticles in primary neural cell cultures are mainly taken up by microglia. *BMC Neurosci*. 2012;13:32.

[51] Cengelli F, Maysinger D, Tschudi-Monnet F, et al. Interaction of functionalized superparamagnetic iron oxide nanoparticles with brain structures. *J Pharmacol Exp Ther*. 2006;318(1):108–116.

[52] Wu HY, Chung MC, Wang CC, Huang CH, Liang HJ, Jan TR. Iron oxide nanoparticles suppress the production of IL-1beta via the secretory lysosomal pathway in murine microglial cells. *Part Fibre Toxicol*. 2013;10:46.

[53] Trickler WJ, Lantz SM, Murdock RC, et al. Silver nanoparticle induced blood-brain barrier inflammation and increased permeability in primary rat brain microvessel endothelial cells. *Toxicol Sci*. 2010; 118(1):160–170.

[54] Huang CL, Hsiao IL, Lin HC, Wang CF, Huang YJ, Chuang CY. Silver nanoparticles affect on gene expression of inflammatory and neurodegenerative responses in mouse brain neural cells. *Environ Res*. 2015;136:253–263.

[55] Crews FT, Vetreno RP. Addiction, adolescence, and innate immune gene induction. *Front Psychiatry*. 2011;2:19

[56] Zorina Y, Iyengar R, Bromberg KD. Cannabinoid 1 receptor and interleukin-6 receptor together induce integration of protein kinase and transcription factor signaling to trigger neurite outgrowth. *J Biol Chem*. 2010;285(2):1358–1370.

[57] Noske W, Lentzen H, Lange K, Keller K. Phagocytotic activity of glial-cells in culture. *Exp Cell Res*. 1982;142(2):437–445.

[58] Geisow MJ, Hart PD, Young MR. Temporal changes of lysosome and phagosome Ph during phagolysosome formation in macrophages—studies by fluorescence spectroscopy. *J Cell Biol*. 1981;89 (3):645–652.

[59] Pickard MR, Jenkins SI, Koller CJ, Furness DN, Chari DM. Magnetic nanoparticle labeling of astrocytes derived for neural transplantation. *Tissue Eng Part C Methods*. 2011;17(1):89–99.

[60] Chen L, Liu L, Yin J, Luo Y, Huang S. Hydrogen peroxide-induced neuronal apoptosis is associated with inhibition of protein phosphatase 2A and 5, leading to activation of MAPK pathway. *Int J Biochem Cell Biol*. 2009;41(6):1284–1295.

[61] Beltran B, Mathur A, Duchen MR, Erusalimsky JD, Moncada S. The effect of nitric oxide on cell respiration: a key to understanding its role in cell survival or death. *Proc Natl Acad Sci USA*. 2000;97(26): 14602–14607.

[62] Dawson VL, Dawson TM, London ED, Bredt DS, Snyder SH. Nitric oxide mediates glutamate neurotoxicity in primary cortical cultures. *Proc Natl Acad Sci USA*. 1991;88(14):6368–6371.

[63] Orr CF, Rowe DB, Halliday GM. An inflammatory review of Parkinson's disease. *Prog Neurobiol*. 2002;68(5):325–340.

SUPPORTING INFORMATION

Additional Supporting Information may be found in the online version of this article.

How to cite this article: Hsiao I-L, Hsieh Y-K, Chuang C-Y, Wang C-F, Huang Y-J. Effects of silver nanoparticles on the interactions of neuron- and glia-like cells: Toxicity, uptake mechanisms, and lysosomal tracking. *Environmental Toxicology*. 2017;00:000–000. https://doi.org/10.1002/tox.22397